Appl. Phys. A (2015) 120:675–681
DOI 10.1007/s00339-015-9237-6

Applied Physics A
Materials Science & Processing

CrossMark

Optical and low-temperature thermoelectric properties of phase-pure p-type InSe thin films

K. S. Urmila[1] · T. A. Namitha[1] · R. R. Philip[2] · B. Pradeep[1]

Received: 7 March 2015 / Accepted: 13 May 2015 / Published online: 20 May 2015
© Springer-Verlag Berlin Heidelberg 2015

Abstract Polycrystalline phase-pure p-type InSe thin films were deposited on glass substrates by reactive evaporation at an optimized substrate temperature of 473 ± 5 K and pressure of 10^{-5} mbar. The as-prepared InSe thin films were analyzed by X-ray diffractometry, energy-dispersive X-ray spectroscopy, atomic force microscopy, UV–Vis–NIR spectroscopy, electrical conductivity and Hall measurements. The lattice parameters, particle size, dislocation density, number of crystallites per unit area and the lattice strain of the prepared InSe thin films were calculated and found as $a = 4.00 \pm 0.002$ Å and $c = 16.68 \pm 0.002$ Å, 48 ± 2 nm, 4.34×10^{10} lines cm^{-2}, 15.37×10^{10} cm^{-2} and 1.8×10^{-3}, respectively. The as-deposited InSe thin films showed a direct allowed transition with an optical band gap of 1.35 ± 0.02 eV and high absorption coefficient of about 10^5 cm^{-1}. The oscillator energy (E_o) and dispersion energy (E_d) were calculated using the single-oscillator Wemple and DiDomenico model. The p-type conductivity and photosensitivity of the as-prepared InSe thin films confirmed their potential application in photovoltaic devices. The mean free path, relaxation time, density of states, Fermi energy and effective mass of holes in the film were determined by correlating the results of thermopower and Hall measurements. The sudden and sharp increase in thermopower from 80 to 37 K was explained as due to the effect of phonon drag on charge carriers.

1 Introduction

Indium monoselenide (InSe) is an important III–VI layered semiconductor extensively studied in recent years due to its promising optical and electrical properties that are suitable for the fabrication of thin film solar cells [1], switching devices [2], radiation detectors [3], Schottky diodes [4] and Li-solid-state batteries [5]. The layered structure of InSe allows the tuning of its electrical properties by means of intercalation so as to suit the processing of various semiconductor devices [6]. Moreover, the absence of dangling bonds on the surface layer makes InSe a promising candidate for application in heterojunction devices [7]. Researchers have successfully demonstrated the growth of InSe heterostructures such as ZnSe/InSe/Si [8], γ-In_2Se_3/TCO (SnO_2 or ZnO) [9] and InSe homojunction p–n photodiodes [10]. The conduction type and optoelectronic properties of InSe thin films are very sensitive to the growth parameters such as rate of evaporation and substrate temperature. Variations in the growth parameters yield different stoichiometric compositions of indium selenide such as InSe, In_2Se_3, In_4Se_3, In_6Se_7 and In_9Se_{11} [11]. InSe thin films can be prepared by several methods including chemical bath deposition [12], flash evaporation [13], metal organic chemical vapor deposition [14], spray pyrolysis [15] and pulsed laser deposition [16].

Recently, Kavitha et al. [12] reported that the mechanical weakness arising from the weak van der Waals force between the layers of InSe hinders the use of InSe crystals in photovoltaic and optoelectronic devices. In order to overcome this difficulty, the preparation of InSe

✉ K. S. Urmila
urmilaks7@gmail.com

[1] Solid State Physics Laboratory, Department of Physics, Cochin University of Science and Technology, Kochi 682022, Kerala, India

[2] Thin Film Research Laboratory, Department of Physics, Union Christian College, Aluva, Kochi 683102, Kerala, India

crystal in the form of thin film has emerged into a subject of active research. But one of the difficulties encountered in the preparation of InSe thin films is the existence of multi-phases in a single film due to the constriction of formation energy range of InSe in the phase diagram of In–Se system [11]. Due to the coexistence of different phases, there is inconsistency in the literature on the properties of InSe thin films even of the same composition. Hence, it is of great significance to study the properties of single-phase InSe thin film in view of its use in solar cells.

Hence, in the present work, an attempt is made to prepare phase-pure p-type InSe thin films by reactive evaporation about which research reports are comparatively less. The as-prepared InSe thin films were characterized by X-ray diffractometry (XRD), energy-dispersive X-ray spectroscopy (EDAX), atomic force microscopy (AFM), UV–Vis–NIR spectroscopy, electrical conductivity and Hall measurements. To the best of our knowledge, this is the first report on the low-temperature thermoelectric power (TEP) properties of single-phase InSe thin films. Moreover, the photosensitivity and dispersion parameters of the films are calculated and the results are interpreted.

2 Materials and methods

Thin films of InSe were prepared by reactive evaporation, a variant of Gunther's three-temperature method [17]. Reactive evaporation is one of the most successful methods used for the industrial-scale production of polycrystalline thin films for high-efficiency solar cells. This technique provides stoichiometric films with excellent reproducibility, uniform deposition, large-area production and high deposition rate. The detailed experimental procedure has been described elsewhere [18]. Briefly, high-purity indium (99.999 %) and selenium (99.99 %) were evaporated simultaneously at suitable rates from two independently heated sources and were allowed to deposit on glass substrates kept at an elevated temperature of 473 ± 5 K. The deposition of thin film was carried out at a pressure of 10^{-5} mbar. The optimized conditions used to deposit InSe thin films for the present work:

Impingement rate of Indium $\approx 3.6 \times 10^{15}$ atoms $cm^{-2}\,s^{-1}$

Impingement rate of Selenium $\approx 3.8 \times 10^{15}$ atoms $cm^{-2}\,s^{-1}$

Substrate temperature: 473 ± 5 K

X-ray diffraction pattern was recorded in the range $2\theta = 5°–70°$ by Rigaku D MaxC X-Ray Diffractometer with Cu-Kα (1.5404 Å) as the radiation source. The composition of the film was analyzed by EDAX (LINK 10000, Cambridge Instruments). The surface morphology of the film was investigated by AFM (AFM nanoscope E, Digital Instruments) employed in contact mode. The optical transmission spectrum of the film was recorded in the wavelength range 190–2500 nm by JASCO V-570 UV–Vis–NIR spectrophotometer. The photocurrent of the sample at room temperature was measured by Keithley 2611A source meter. An FSH lamp (82 V, 300 W) was used as the source of illumination. The variation of electrical conductivity of the sample with temperature was studied in the range 300–423 K at intervals of 5 K for three continuous heating and cooling cycles by DC four-probe method. The measurement was carried out in a conductivity cell at a pressure of 10^{-3} mbar. Hall measurement (Van der Pauw ECOPIA HMS-3000 system) was performed at room temperature by placing the film in a magnetic field of 8000 G and measuring the current–voltage characteristics by DC four-probe method. The thickness of the film was ~ 170 nm, measured by Veeco Dektak 6M Stylus Profiler. The p-type conductivity of the prepared film was determined by hot-probe method.

Thermoelectric power (TEP) measurement was carried out in the temperature range of 4–300 K using liquid helium as the coolant. Ohmic electrodes were drawn on the sample using silver paste. The sample was placed between two oxygen-free highly conducting (OFHC) copper blocks. The details of the experimental setup are given in Ref. [19].

3 Results and discussion

3.1 Structural analysis

Figure 1 shows the XRD pattern of the prepared phase-pure InSe thin film.

The diffraction peaks were indexed using the Joint Committee on Powder Diffraction Standards (JCPDS) and

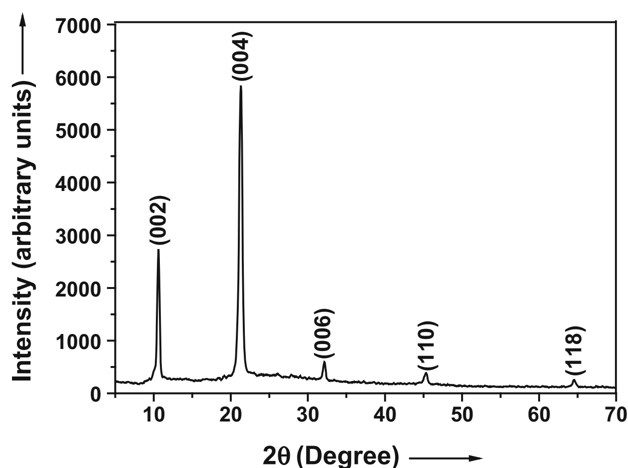

Fig. 1 XRD pattern of the prepared phase-pure InSe thin film

matched with (JCPDS card no. 34-1431). The prepared films were polycrystalline in nature and showed a well-defined peak at $2\theta = 21.30°$ corresponding to the (004) plane of InSe with hexagonal structure (JCPDS card no. 34-1431). No characteristic peaks of elemental In/Se were observed in the XRD pattern. No peaks corresponding to other secondary phases of indium selenide such as In_2Se_3, In_4Se_3, In_6Se_7 and In_9Se_{11} were observed either. These results confirmed the formation of single-phase or phase-pure InSe thin film. The lattice parameters of the InSe were calculated as $a = 4.00 \pm 0.002$ Å and $c = 16.68 \pm 0.002$ Å. These calculated values of lattice parameters very well matched with those listed in the JCPDS card no. 34-1431. The average crystallite size of the prepared InSe thin film was calculated using Scherrer equation [20] and was obtained as 48 ± 2 nm. The microstructural parameters such as dislocation density, number of crystallites per unit area and lattice strain in the film were estimated as 4.34×10^{10} lines cm^{-2}, 15.37×10^{10} cm^{-2} and 1.8×10^{-3}, respectively [18].

3.2 Compositional and morphological analysis

Figure 2 shows the EDAX spectrum of the prepared InSe thin film. The average atomic percent of In and Se in the sample was determined as 49.45 % and Se = 50.55 %, respectively, indicating the near stoichiometric composition of the InSe thin film.

Figures 3 and 4 show the two-dimensional (2D) and three-dimensional (3D) AFM images of the prepared InSe thin film. The scan rate was 10.172 Hz, and scan area was 2 µm × 2 µm. It can be seen from Fig. 3 that the film exhibited clusters of sizes in the range 200–300 nm in diameter, indicating agglomeration of particles. The root mean square (RMS) surface roughness of the sample determined from 3D AFM image was ~20 nm, suggesting a significantly smooth surface.

3.3 Optical analysis

The optical band gap, absorption coefficient and optical constants of the as-prepared film were evaluated from the transmission spectrum depicted in Fig. 5b using Swanepoel's method [21]. The absorption coefficient (α) showed a high value of about 10^5 cm^{-1}, suggesting the possible use of the film as absorber layers in solar cells. The optical band gap of the film was determined using the well-known Tauc relation [18]. Figure 5a illustrates the $(\alpha h\nu)^2$ versus $h\nu$ plot of phase-pure InSe thin film.

As can be seen from Fig. 5a, the film showed a direct allowed transition with an optical band gap of 1.35 ± 0.02 eV. The band gap thus obtained was in good agreement with 1.3 eV reported for single-crystal InSe [22] and was also well within the optimum range for harvesting solar energy. In order to determine the structural disorder that occurred in the film during its formation, the Urbach energy E_U [23] of the film was calculated from the inverse of slope of the plot of ln(α) versus $h\nu$ shown in Fig. 5c. E_U was obtained as 0.5 eV, a small value which indicates less structural disorder.

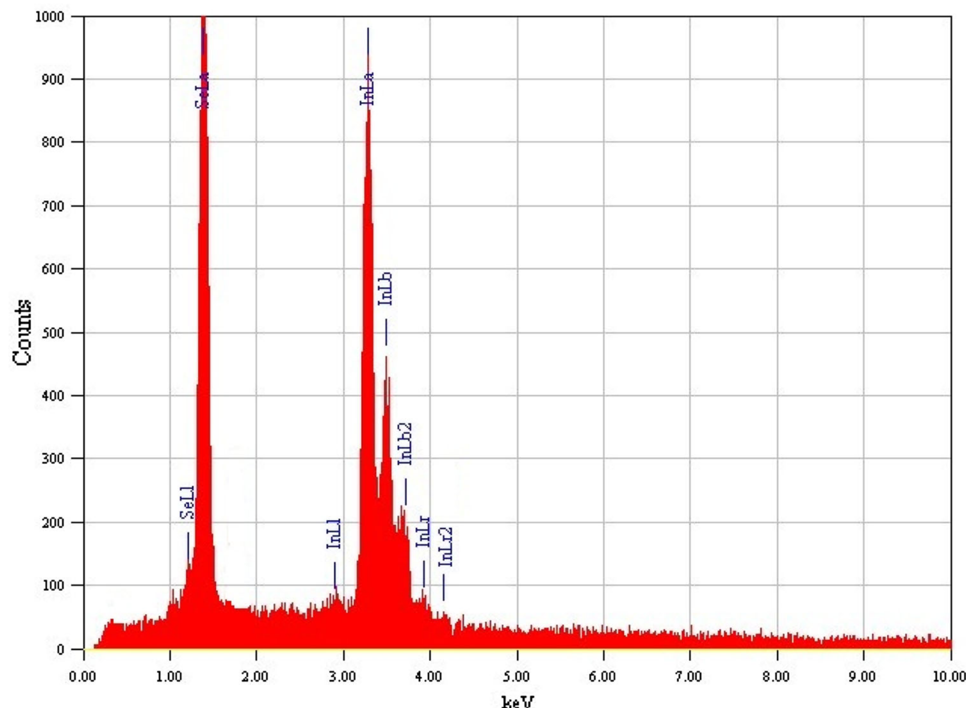

Fig. 2 EDAX spectrum of phase-pure InSe thin film

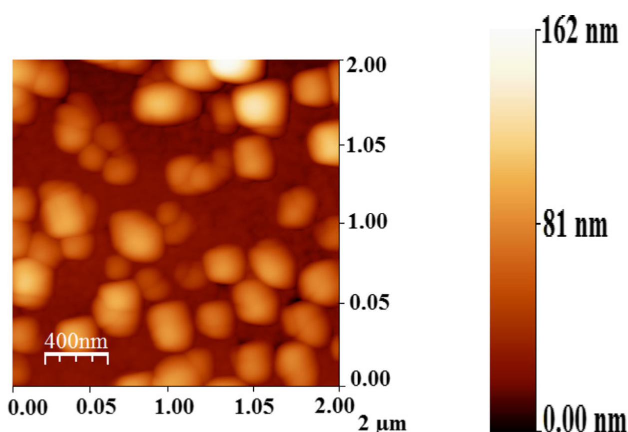

Fig. 3 2D AFM of InSe thin film

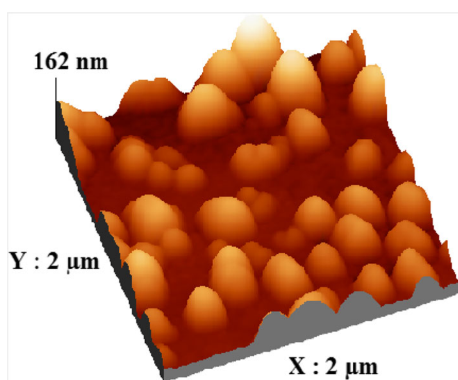

Fig. 4 3D AFM of InSe thin film

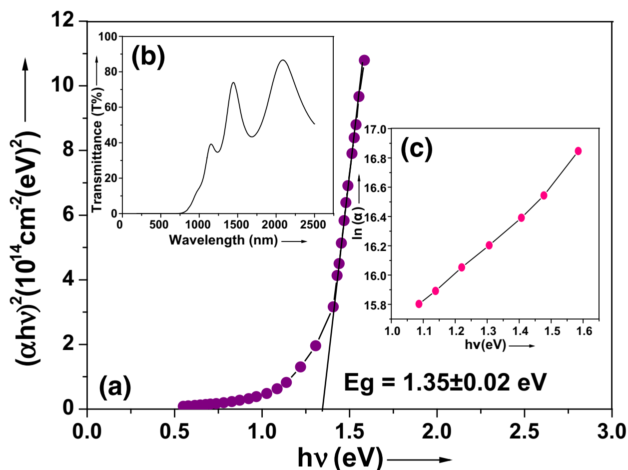

Fig. 5 Plots of **a** $(\alpha h\nu)^2$ versus $h\nu$, **b** transmission spectrum and **c** $\ln(\alpha)$ versus $h\nu$ of phase-pure InSe thin film

The refractive index (n), extinction coefficient (k), the real part (ε_1) and imaginary part (ε_2) of the dielectric constant [24] of the prepared film were calculated using Swanepoel's method [21], and their dependence on photon energy is presented in Fig. 6.

The high refractive index and low extinction coefficient of the prepared film can be attributed to its better crystalline nature. This assumption was in accordance with the results reported by Senthil et al. [25] for vacuum-evaporated CdS thin films of grain size 24 nm. Furthermore, it was clear from Fig. 6 that ε_1 varied with photon energy in a similar manner as that of n, whereas ε_2 varied with photon energy in a similar manner as that of k. Hence, ε_1 can be related to dispersion and ε_2 can be related to the extinction coefficient k.

The spectral dependence of the refractive index of the film was further analyzed using Wemple and DiDomenico (WD) model [26]. According to WD model, the dispersion of refractive index is given by

$$n^2 - 1 = \frac{E_o E_d}{E_o^2 - (h\nu)^2} \quad (1)$$

where E_o is the single-oscillator energy (average of optical band gap) and E_d is the dispersion energy (measure of strength of interband optical transitions) [16]. The parameters E_o and E_d were determined from the plot of $(n^2-1)^{-1}$ versus $(h\nu)^2$ shown in Fig. 7. The E_o and E_d values of the prepared film were calculated as 2.58 and 17.96 eV, respectively. The oscillator energy was found to be two times the optical band gap ($E_o \approx 2E_g$) [27].

3.4 Electrical conductivity and photoconductivity measurements

The positive value of Hall coefficient confirmed the p-type conductivity of the film. The sample showed a hole concentration $p \sim 9.8 \times 10^{16}$ cm^{-3}, hole mobility $\mu_h \sim 12.5$ cm^2 V^{-1} s^{-1} and electrical conductivity $\sigma \sim 0.2\ \Omega^{-1}$ cm^{-1} at room temperature.

The increase in current with temperature shown in Fig. 8 revealed the semiconducting behavior of the deposited film. The activation energy was calculated from the slope of $\ln(I)$ versus $1000/T$ plot [28] and was obtained as 0.11 ± 0.01 eV.

Figure 9 illustrates the photoresponse curve of InSe thin film. The measurement was performed at room temperature, first in the dark followed by illumination of the sample and then after cutting off illumination. The photosensitivity (PS) of the film is defined as

$$PS = \frac{I_L - I_D}{I_D} \quad (2)$$

where I_L is the current under illumination and I_D is the dark current [29]. The room temperature photosensitivity of the prepared InSe thin film was calculated as 0.5 ± 0.02.

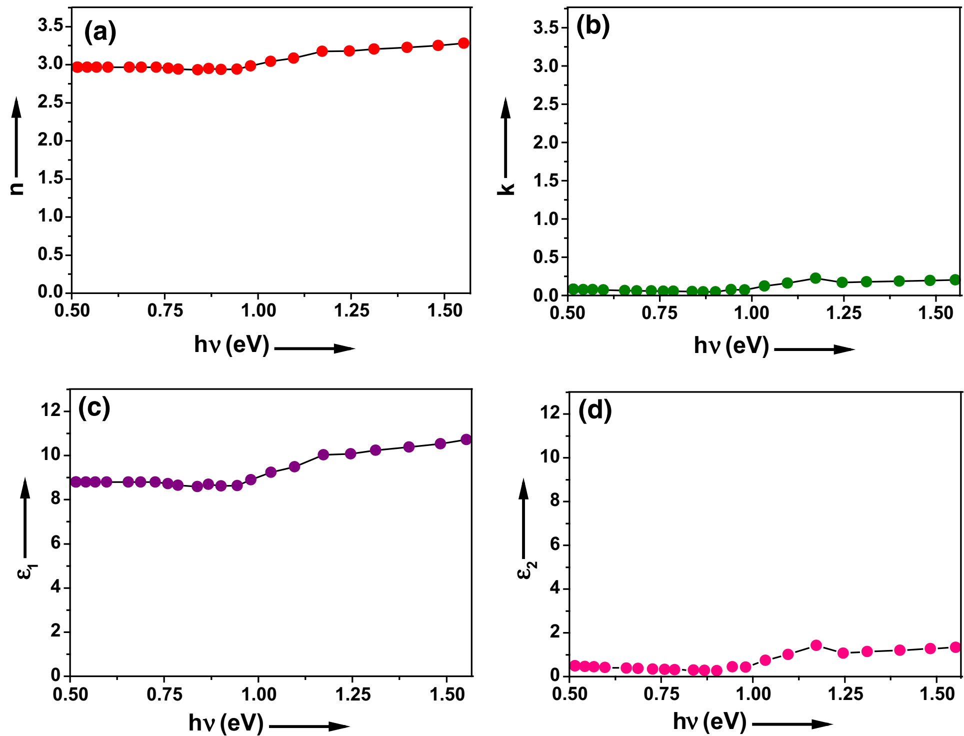

Fig. 6 Variations of **a** n, **b** k, **c** ε_1 and **d** ε_2 with photon energy

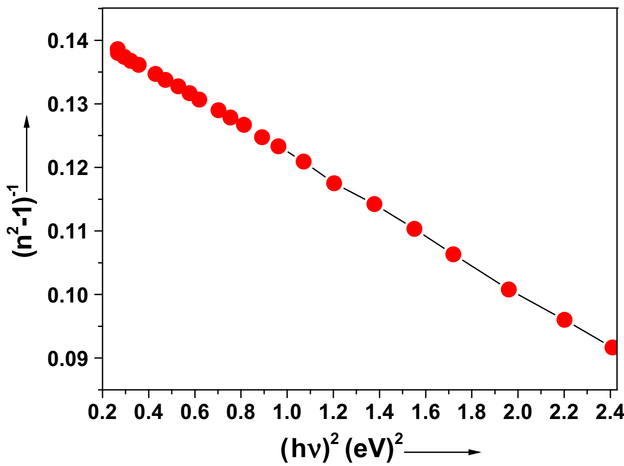

Fig. 7 Plot of $(n^2 - 1)^{-1}$ versus $(h\nu)^2$

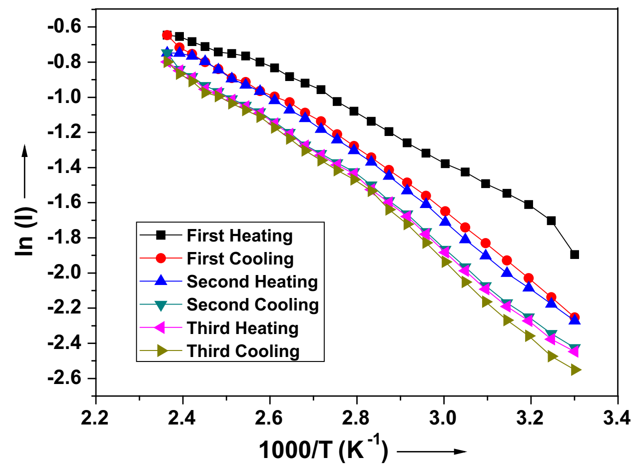

Fig. 8 Variation of ln(I) with inverse of temperature of InSe thin film

The increase in photocurrent on illumination was due to generation of electron hole pairs in the film, and it indicated the photoconducting nature of the prepared film.

3.5 Low-temperature TEP measurements

Figure 10 depicts the variation of TEP with temperature of InSe thin film.

The positive values of TEP indicated that the prepared thin films are of p-type. The variation of TEP with temperature shown in Fig. 10 confirmed the semiconducting nature of the film. The Seebeck coefficient (S) depends on temperature as

$$S = \pm \frac{K_B}{e}\left[A + \frac{E_F}{K_B T}\right] \quad (3)$$

where E_F is the separation of Fermi level from the top of the valence band edge, K_B is the Boltzmann constant, T is the temperature at which thermoelectric power is determined, and A is the scattering parameter [30]. By using Eq. (3), the position of Fermi level was determined as $\sim$0.02 eV above the valence band. The value of A was

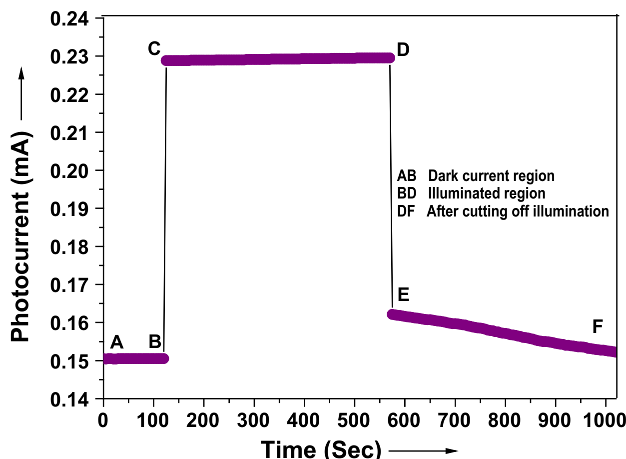

Fig. 9 Photoresponse curve of InSe thin film at room temperature

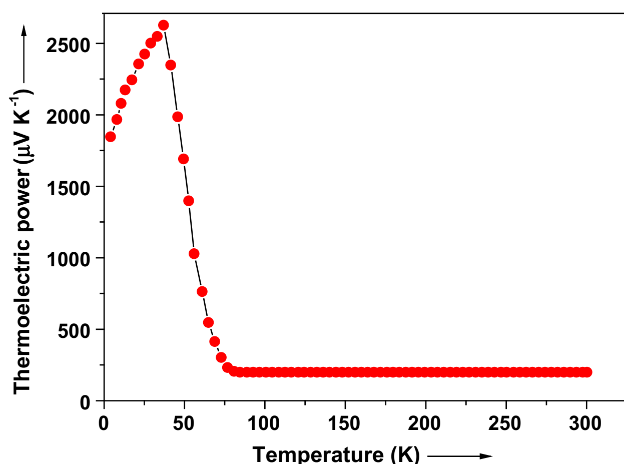

Fig. 10 Variation of TEP with temperature of InSe thin film

obtained as 3/2, indicating ionized impurity scattering [31]. The effective mass of holes m_h^* was calculated by using the equations

$$p = N_{\mathrm{V}} \exp\left[-\left(\frac{E_{\mathrm{F}} - E_{\mathrm{V}}}{K_{\mathrm{B}} T}\right)\right] \quad (4)$$

$$N_{\mathrm{V}} = 2\left(\frac{2\pi m_h^* K_{\mathrm{B}} T}{h^2}\right)^{3/2} \quad (5)$$

where N_{V} is the effective density of states at the valence band edge, K_{B} is the Boltzmann constant, T is the temperature, and h is the Planck's constant [32]. The values of N_{V} and m_h^* were obtained as $\sim 5.7 \times 10^{17}\ \mathrm{cm}^{-3}$ and $\sim 0.08\ m_0$, respectively, where m_0 is the rest mass of electron. The relaxation time (τ) and a mean free path (λ) of charge carriers in the film were evaluated as $\sim 5.7 \times 10^{-16}$ s and ~ 0.17 nm, respectively. Hence, a deeper knowledge of the material properties can be achieved by correlating the results of TEP and Hall measurements.

As can be seen from Fig. 10, the thermoelectric power (S) was constant up to 83 K. But as the temperature was lowered from 83 K, there was a sudden and sharp increase in S whose onset was at around 80 K and a peak was observed at 37 K. The prepared InSe thin film exhibited a reasonably high-positive thermoelectric power $2626 \pm 2\ \mu\mathrm{VK}^{-1}$ at 37 K. In the present study, the rapid increase in thermoelectric power observed at low temperatures (80–37 K) has been attributed to the effect of phonon drag on charge carriers resulting from the interaction of phonons with mobile carriers [33]. Therefore, the thermoelectric term S can be expressed as $S = S_e + S_g$, where S_e results from the diffusion of charge carrier from hot to cold end and S_g results from the drag on charge carriers by the phonons moving from hot to cold end [33]. It can also be seen from Fig. 10 that, as the temperature was lowered from 37 K, S showed a decrease and attained a value of $1846 \pm 2\ \mu\mathrm{VK}^{-1}$ at 4 K. This decrease in S is due to the fact that below about one-fifth of Debye temperature (θ_{D}), there are not enough phonons available for drag. As a result, the phonon drag effect to thermoelectric power was greatly weakened, which led to a decrease in thermopower. θ_{D} for InSe is 190 K [34]. Thus, in the temperature range of 300–83 K, the main contribution to TEP was from electrons. On the other hand, in the temperature range of 80–37 K, the thermal vibrations of the lattice played a dominant role in raising the value of TEP—a phenomenon usually observed for specimens of high to moderate resistivity [33]. To the best of our knowledge, this is the first report to investigate the low-temperature TEP properties of phase-pure InSe thin films, and hence, it is not possible to present a comparative study of our results with the literature. The InSe film showed a considerably high Seebeck coefficient $2626 \pm 2\ \mu\mathrm{VK}^{-1}$ at 37 K, which on further work can possibly open up new advances in the field of cryogenic thermoelectric materials.

4 Conclusions

Phase-pure polycrystalline InSe thin films were successfully deposited on glass substrates by the simultaneous evaporation of constituent elements under optimized deposition conditions using a modified form of Gunther's three-temperature method. The near-optimum band gap for harvesting solar energy, high absorption coefficient and reasonable photosensitivity of reactive-evaporated phase-pure InSe thin film confirmed its possible use as absorber material in solar cells. Temperature variation of TEP suggested the semiconducting nature of the film with p-type conduction. The effective mass of hole was determined as $\sim 0.08\ m_0$ with position of Fermi level at ~ 0.02 eV above the valence band. The observed sudden and sharp increase

in TEP from 80 to 37 K was explained as the effect of phonon drag on charge carriers. On further work, the prepared films can also be considered for low-temperature thermoelectric applications because of its considerably high Seebeck coefficient 2626 ± 2 μVK^{-1} at 37 K.

Acknowledgments K. S. Urmila would like to thank University Grants Commission (UGC), Government of India, for financial assistance in the form of Research Fellowship in Science for Meritorious Students (RFSMS). R. R. Philip acknowledges Department of Science and Technology (DST), Government of India, for funding a major project. Thanks are also due to Dr. V. Ganesan and Dr. G. S. Okram of UGC-DAE Consortium for Scientific Research, Indore, India, for providing AFM and TEP facilities.

References

1. G. Gordillo, C. Calderon, Sol. Energy Mater. Sol. Cells **77**, 163 (2003)
2. M.A. Kenawy, A.F.E. Shazly, M.A. Afifi, H.A. Zayed, H.A.E. Zahid, Thin Solid Films **200**, 203 (1991)
3. V.M. Koshkin, L.P. Galchinetskii, V.N. Kulik, B.I. Minkov, U.A. Ulmanis, Solid State Commun. **13**, 1 (1973)
4. P. Matheswaran, R. Sathyamoorthy, K. Asokan, Electron. Mater. Lett. **8**, 621 (2012)
5. M. Balkanski, P.G.D. Costa, R.F. Wallis, Phys. Status Solid. B **194**, 175 (1996)
6. V.B. Boledzyuk, Z.D. Kovalyuk, M.N. Pyrlya, Inorg. Mater. **45**, 1222 (2009)
7. T. Matsushita, T.T. Nang, M. Okuda, A. Suzuki, S. Yokota, Jpn. J. Appl. Phys. **15**, 901 (1976)
8. B. Ullrich, Mater. Sci. Eng., B **56**, 69 (1998)
9. S. Marsillac, J.C. Bernede, Thin Solid Films **315**, 5 (1998)
10. Z.D. Kovalyuk, V.N. Katerynchuk, O.A. Politanska, O.N. Sydor, V.V. Khomyak, Tech. Phys. Lett. **31**, 359 (2005)
11. H. Okamoto, J. Phase Equilib. Diff. **25**, 201 (2004)
12. B. Kavitha, M. Dhanam, J. Ovonic Res. **6**, 75 (2010)
13. M. Persin, A. Persin, B. Celustka, B. Etlinger, Thin Solid Films **11**, 153 (1972)
14. S.S. Lee, K.W. Seo, I.W. Shim, Bull. Korean Chem. Soc. **27**, 147 (2006)
15. H. Bouzouita, N. Bouguila, S. Duchemin, S. Fiechter, A. Dhouib, Renew Energ. **25**, 131 (2002)
16. M. Hrdlicka, J. Prikryl, M. Pavlista, L. Benes, M. Vlcek, M. Frumar, J. Phys. Chem. Solids **68**, 846 (2007)
17. K.G. Gunther, in *The use of thin films in physical investigations*, ed. by J.C. Anderson (Academic press, London, 1966), p. 213
18. K.S. Urmila, T.A. Namitha, R.R. Philip, V. Ganesan, G.S. Okram, B. Pradeep, Phys. Status Solid. B **251**, 689 (2014)
19. A. Soni, G.S. Okram, Rev. Sci. Instrum. **79**, 1251031 (2008)
20. B.D. Cullity, in *Elements of X-ray diffraction*, ed. by M. Cohen (Addison-Wesley, Philippines, 1978), p. 81
21. R. Swanepoel, J. Phys. E: Sci. Instrum. **16**, 1214 (1983)
22. A. Mandelis, in *Handbook of optical constants of solids*, ed. by E.D. Palik (Academic Press, USA, 1998), p. 59
23. F. Urbach, Phys. Rev. **92**, 1324 (1953)
24. T.S. Moss, G.J. Burrell, B. Ellis, *Semiconductor opto-electronics*, 1st edn. (Butterworths, London, 1973), pp. 23–47
25. K. Senthil, D. Mangalaraj, S.K. Narayandass, S. Adachi, Mater. Sci. Eng., B **78**, 53 (2000)
26. S.H. Wemple, M. DiDomenico, Phys. Rev. B **3**, 1338 (1971)
27. A. Larbi, H. Dahman, M. Kanzari, Vacuum **110**, 34 (2014)
28. E.S.M. Farag, M.M. Sallam, Egypt. J. Solids. **30**, 1 (2007)
29. R.K. Murali, P. Thirumoorthy, ECS Trans. **28**, 67 (2010)
30. H.B. Kwok, R.H. Bube, J. Appl. Phys. **44**, 138 (1973)
31. R.A. Smith, *Semiconductors*, 1st edn. (Cambridge University Press, Cambridge, 1959), pp. 291–371
32. N.D. Gupta, A.D. Gupta, in *Semiconductor devices: modelling and technology*, ed. by A.K. Ghosh (Prentice Hall of India, New Delhi, 2004), p. 1
33. C. Herring, Phys. Rev. **96**, 1163 (1954)
34. O. Madelung, *Semiconductors: Data Handbook*, 3rd edn. (Springer, Berlin, 2004), pp. 515–552